WARSAW UNIVERSITY OF TECHNOLOGY Index 351733
FACULTY OF CIVIL ENGINEERING
COMMITTEE FOR CIVIL AND WATER ENGINEERING
POLISH ACADEMY OF SCIENCES ISSN 1230-2945

DOI: 10.24425/ace.2020.136484

ARCHIVES OF CIVIL ENGINEERING

Vol. LXVII ISSUE 1 2021

© 2021. R. Chmielewski, L. Kruszka, R. Rekucki, K. Sobczyk.

This is an open-access article distributed under the terms of the Creative Commons Attribution-NonCommercial-NoDerivatives License (CC BY-NC-ND 4.0, https://creativecommons.org/licenses/by-nc-nd/4.0/), which per-mits use, distribution, and reproduction in any medium, provided that the Article is properly cited, the use is non-commercial, and no modifications or adaptations are made.

EXPERIMENTAL INVESTIGATION OF DYNAMIC BEHAVIOR OF SILTY SAND

R. CHMIELEWSKI[1], L. KRUSZKA[2], R. REKUCKI[3], K. SOBCZYK[4]

Abstract: The paper includes experimental research using the Split Hopkinson Pressure Bar to determine dynamic compression curves and strength dynamic parameters to depend on the strain rate and moisture for silty sand soil samples. Those experiments are oedometric type based in a rigid confining cylinder. Samples of silty sand with fine a fraction content were taken for the study. To ensure sufficiently uniaxial strain of the tested material, the soil samples were placed in properly prepared casings made of duralumin for the needs of the tests. Thanks to the use of measuring strain gauges on the initiating and transmitting bars, as well as the casing, the nature of the loading pulse was obtained, which was then subjected to the process of filtration and data processing to obtain the nature of the incident, reflected and transmitted wave. During the above dynamic experiments with the representative of silty sand soils, it was observed that its dynamic compaction at a high strain rate is different than in the case of the Proctor test. This is due to higher compaction energy, which additionally changes the grain size by destroying the grains in the structure. The paper presents the results of particle size distribution analysis for two different types of soil samples - this type of analysis is unique. Hence experiments should be further continued for such soils with different granulations and various moisture using, for example, Hopkinson measuring bar technique to confirm for other silty sand soils that are often subgrade of various engineering objects.

Keywords: soil mechanics, experimental dynamic testing, split Hopkinson pressure bar, oedometric test.

[1] Lt Col, Ph. D., email: ryszard.chmielewski@wat.edu.pl, Military Univ. of Technology, Dept. of Military Engineering and Military Infrastructure, 2 Gen. Sylwester Kaliski Str., 00-908 Warsaw, Poland

[2] Ph.D., email: leopold.kruszka@wat.edu.pl (corresponding author), Military Univ. of Technology, Dept. of Military Engineering and Military Infrastructure, 2 Gen. Sylwester Kaliski Str., 00-908 Warsaw, Poland

[3] M. Sc., email: ryszard.rekucki@wat.edu.pl, Military Univ. of Technology, Dept. of Military Engineering and Military Infrastructure, 2 Gen. Sylwester Kaliski Str., 00-908 Warsaw, Poland

[4] Lt, M. Sc., email: kamil.sobczyk@wat.edu.pl, Military Univ. of Technology, Dept. of Military Engineering and Military Infrastructure, 2 Gen. Sylwester Kaliski Str., 00-908 Warsaw, Poland

1. INTRODUCTION

For many years, the unflagging interest and continuous development in the field of testing the mechanical properties of various building materials subjected to dynamic effects stresses have been noticed [1]. Particularly significant increase in the number of publications in this field concerns metals as well as for concretes [2], polymers, wood and soils [3-18]. Indeed, a large part of engineering problems includes research into high-rate strain-stress (HSR) soil response. This includes stress related to, inter alia, explosions [19-21], earthquakes, mine explosions [22], wheel loads of vehicles and aircrafts [23], dynamic soil compaction [24] and pile driving [25]. This is associated with the need to create as true and correct as possible constitutive models that are important in the process of calculating geoengineering properties as part of computer-aided design methods. It should be noted that in the process of constitutive modeling it is necessary to know the quasi-static and dynamic characteristics in a wide range of high strain rates together with changes in the physical characteristics of the soils subjected to this type of impact.

In tests using standard testing machines, it is possible to determine the strength parameters of materials for strain rates up to 5 [s^{-1}]. On the other hand, dynamic tests, require special testing equipment. John Hopkinson and his son Bertram Hopkinson are considered precursors in the field of material research methodology within high strain rates [26-28]. As a result of further works, Herbert Kolsky presented an experimental method called the Kolsky method or the Hopkinson bar technique for the range of strain rates from $5 \cdot 10^2$ [s^{-1}] up to $5 \cdot 10^4$ [s^{-1}] [29]. Due to the fact that soil is characterized by low stiffness, low impedance and high attenuation of waves, conventional test equipment typical for other materials is not suitable and should be modified depending on the needs in terms of adaptation to the soil sample. Soil behaviour during uniaxial dynamic compression has been studied in detail for matching of the soil sample.

Currently, in modern laboratories for dynamic soil testing, a test device called the Split Hopkinson Pressure Bar (SHPB) is used, operating on the basis of two measuring bars (initiating and transmitting) along with the tested soil sample placed between these bars. To determine the strain rate above $5 \cdot 10^4$ [s^{-1}] (the study for other materials than soil was published in [30, 31]), an additional modification of the Hopkinson Pressure Bar is used by exclusion of the initiating bar from the system and a direct impact with the bar-projectile on the sample adjacent to the transmitting bar (modification of the Hopkinson bar by applying a direct impact with loading bar-projectile on sample adhering to transmitting bar).

This paper presents the results of experimental tests using the SHPB to determine the strength dynamic parameters of silty sand soil samples with different moisture content subjected to dynamic impact under the condition of limiting its radial deformation. It should be also mentioned here that are well-known versions of the Kolsky method for determining the radial stress component in the specimen tested [5, 6].

2. SOIL AND RESEARCH METHODOLOGY

2.1. Soil specification

Silty sand (siSa) with a fine fraction content, understood as the sum of the silty and argillaceous fractions 20,46 [%] (with a diameter less than 0,063 [mm], $f_i + f_\pi$). The granulation analysis was performed using the wet sieve method with the addition of a curve for fine fractions by the aerometric method. Figure 1 shows the granulation curve of the soil tested.

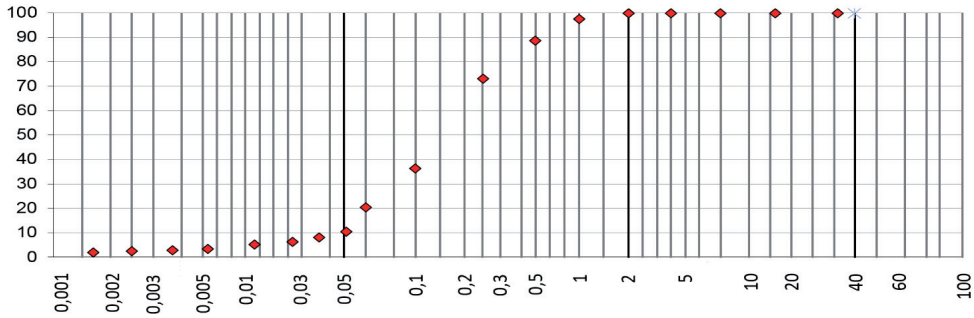

Fig. 1. Granulation curve of the tested soil.

Compactibility parameters ρ_{ds} and w_{opt} determined in the Proctor test, compacting the soil using method I according to the standard [1], (normal method). Figure 2 presents the diagram of the optimum moisture content of the tested soil.

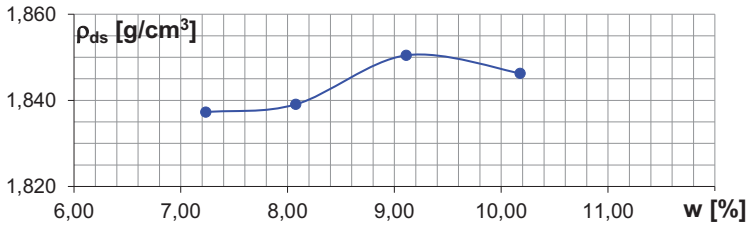

Fig. 2. Diagram of optimal moisture content of the tested soil.

The optimum moisture content of the tested soil was OMC = 9,6 [%], the maximum bulk density of the granular soil structure MDD = 1,86 [g/cm^3]. The aim of the study was to determine the characteristic strength parameters for ground base samples with different moisture content subjected to dynamic impact. Four soil samples were prepared containing percentage of moisture content respectively: $w_1 = 0$ [%], $w_2 = 4{,}6$ [%], $w_3 = 9{,}6$ [%] and $w_4 = 14{,}6$ [%]. Each of them had a length $L_0 \approx 3$ [cm], and the test for individual moisture content of the samples was repeated twice, the results presented are the arithmetic mean of these tests. The samples were placed in casings (which sufficiently ensured the occurrence of uniaxial strain of the tested material) and pressed on both sides with the initiating and transmitting bar.

2.2. Experimental setup

In order to determine the characteristic parameters of the soil samples tested, which were subjected to dynamic strain with a high strain rate, dynamic compression of these samples was performed as part of the test stand based on the Split Hopkinson Pressure Bar (SHPB). The SHPB stand used in the present research, included in this paper, is located in the structure testing workshop on the explosive impact of the Faculty of Civil Engineering and Geodesy (Military University of Technology in Warsaw), its view is shown in Figure 3.

Fig. 3. SHPB test stand. Mechanical part of the station: (1) - pneumatic cannon with a barrel of loading bar-projectile, (2) - initiating measuring bar, (3) - transmitting measuring bar, (4) - soil sample in the casing, (5) - damper. Measuring part: (6) - strain gauges, (7) - compensating strain gauges, (8) - measuring device with digital memory, (9) - laser timekeeping system, (10) - computer software.

The bar-projectile is driven by the rapidly released air pressure from a pneumatic cannon powered by a compressor (1). During the flight of the bar-projectile, the laser timekeeping system (9) reads

the time in which the bar-projectile covers the distance 0,1 $[m]$. Knowing the flight time of the bar-projectile allows determining the speed of the bar-projectile at the moment of impact. After hitting the initiating bar (2), an elastic compression wave develops in it along the bar towards the sample (4). When it reaches the end of the initiating bar, the wave partially continues to propagate through the sample towards the transmitting bar (3), is partly reflected and starts returning to the beginning of the initiating bar. The wave that passed through the sample and reached the transmitting bar at its end is finally amortized (suppressed) (5). The described phenomena are presented in Figure 4.

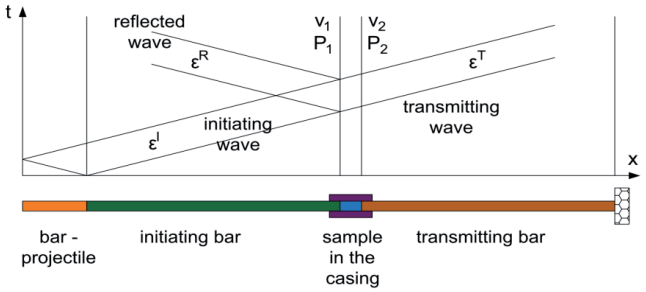

Fig 4. Wave chart illustrating the phenomenon of elastic wave propagation in a Split Hopkinson Pressure Bar. t - time, x - bar axis: bar-projectile and measuring bar, $\varepsilon^I(t), \varepsilon^T(t), \varepsilon^R(t)$ - elastic strain of the measuring bars over time measured by strain gauges, $P_1(t)$ and $P_2(t)$ - dynamic forces at the ends of the tested sample, $v_1(t)$ and $v_2(t)$ - the velocity of the fronts of the measuring bars.

Both on the initiating and transmitting bars, along the axis of the bars, 0,5 [m] from the front of these bars, two active strain gauges (6), parallel to each other, were glued. 1-LY11-3/120A strain gauges were used 3 $[mm]$, of length, resistance $R = 120\ [\Omega] \pm 0{,}35\ [\%]$ and characteristic constant value of the load cell $k = 2{,}02 \pm 1\ [\%]$). Thanks to this solution, the reliability of measurements increased and the impact of undesirable phenomena, e.g. buckling due to the effect of compressive force, was reduced. Active strain gauges glued on the bars, after supplementing with two compensating strain gauges (7) of the same parameters, were included in a full Wheatstone type strain gauge bridge supplied with DC 5 [V] from the LTT24 device (measuring device with digital memory). Part of the incident wave is reflected from the front of the bar and while returning it has a stretchy character. The diagram shows that initially the loading pulse is a positive sign (compression), while the returning wave has a negative sign (stretching). An example of its shape and character is shown in Figure 5. The measurement signals come from 3 channels of the LTT24 measuring device recording changes on active strain gauges included in the full-bridge systems:

- channel 1 - initiating bar;

- channel 2 - transmitting bar;
- channel 3 - sample casing.

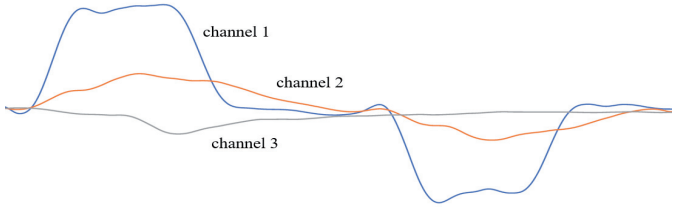

Fig. 5. Samples of recorded pulse shapes from three measurement channels.

On the duralumin casing of the soil sample, whose task due to its thickness is to ensure uniaxial strain of the tested soil, 2 strain gauges were also placed to observe the behaviour of the sample (strain gauges type 1-LY11-3/120A of length 3 $[mm]$, resistance $R = 120\ [\Omega] \pm 0{,}35\ [\%]$) and a strain gauge constant $k = 2{,}02 \pm 1\ [\%]$). Initially, the soil sample is being plastically deformed, which is accompanied by the phenomenon of force balancing P_1 and P_2 at its ends until a homogeneous stress condition is achieved within the sample. Impulses from the strain gauges are recorded using a multi-channel conditioner and LTT24 recorder (8), as well as a dedicated computer software (10). The recording of individual measurement signals was carried out during the experiments as digital signals at a sampling frequency of 1 [MHz] and a 24 bit linear quantization accuracy. Then, the recorded digital signals with a length of 4096 samples were filtered using FlexPro software. The best effects were obtained by low-pass filtration using the Chebyshev window at a cut-off frequency of 55 [kHz]. After filtering, the voltage signals were scaled to a strain unit μm / m. Then, using the appropriate equations and correlations, you can determine the soil sample stress, soil sample strain, soil sample strain rate, as well as the stress in the sample casing depending on time.

A 200 [mm] long bar-projectile and initiating and transmitting bars 1000 [mm] in length and a diameter of 20 [mm] each, were used for the tests. These elements were made of C350 steel characterized by a 200 [GPa] longitudinal modulus and a wave propagation velocity corresponding to the sound speed in the material 5000 [m/s].

The casings are made of duralumin (PA6/EN AW-2017A), which is characterized by a longitudinal elastic modulus of 72,5 [GPa], 27,2 [GPa] transverse modulus and 5100 [m/s] wave propagation velocity. Four casings were prepared - each with an internal diameter of 20 [mm] and an external diameter of 40 [mm] (wall thickness 10 [mm]).

During the tests, efforts were made to implement the assumed equal conditions: pressure of the pneumatic gun at the time of the shot $p \approx 5\ [bar]$, air temperature $T_{air} \approx 20$ [°C] and air humidity $w_{air} \approx 50$ [%] for each experiment carried out.

2.3. Dynamic measurement methodology

To be able to analyse the process of propagation of one-dimensional wave in the longitudinal direction of an infinitely long bar, it must be assumed that it is divided into constituent elements of small dimensions dx. Using the Hooke's law and Newton's second law, the wave propagation equation can be written as follows:

$$\frac{\partial^2 u}{\partial x^2} = \frac{1}{{c_0}^2} \cdot \frac{\partial^2 u}{\partial t^2}; \tag{2.1}$$

where: u - movement within the bar;
c_0 - elastic wave propagation velocity in the longitudinal direction of the bar.

$$c_0 = \sqrt{\frac{E}{\rho}}; \tag{2.2}$$

where: E - Young's Modulus of the material from which the bars are made;
ρ - the density of the material from which the bars are made.

Figure 6 illustrates the propagation of an elastic wave in a bar as a result of a bar-projectile impact towards its longitudinal axis.

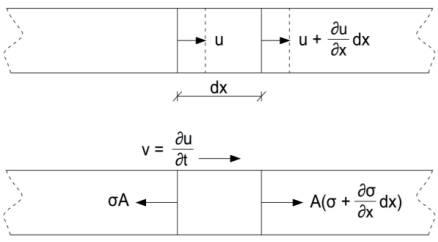

Fig. 6. Diagram of elastic wave propagation in a measuring bar [5].

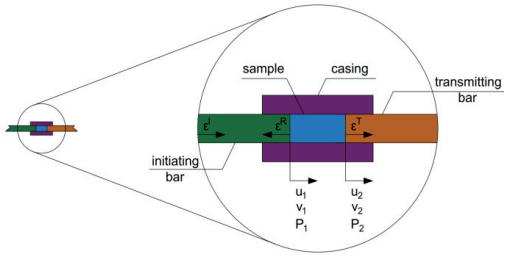

Fig. 7. Contact of the sample with the fronts of both measuring bars.

Further transformations and solutions of equations in this area were well presented in the study [5]. As part of the test, a soil sample was placed between the bars. This experiment is oedometric type, and allows the measurement of the complete three-dimensional dynamic response of soils, where $\sigma_1 = \sigma_x;\ \sigma_2 = \sigma_3 = \sigma_r;\ \varepsilon_1 = \varepsilon_x;\ \varepsilon_2 = \varepsilon_3 = 0$, including also Poisson's ratio $v(t)$ and volumetric strain $\theta = \varepsilon_x$ as functions of time [8, 32]. Based on the knowledge of the incident, passing

and reflected wave characteristics, it is possible to determine the displacement of the sample contact with the bar ends, in Figure 7 marked as u_1 and u_2. The uniaxial strain state ε was also determined in the bars for the initiating wave - ε^I, the transmitting wave - ε^T and the reflected wave - ε^R.

Assuming that a negative sign refers to for the compression wave, we obtain the strain equation:

$$\frac{\partial u}{\partial t} = -c_0 \cdot \varepsilon. \tag{2.3}$$

In the case when the bar-projectile hits the bars at speed v, and the cross-sections and material of the bar-projectile and bars are the same ($A = A_1 = A_2;\ \rho = \rho_1 = \rho_2;\ c_0 = c_1 = c_2$) the maximum stress in the bar σ defines the equation:

$$\sigma = \frac{1}{2} \cdot \rho \cdot c_0 \cdot v. \tag{2.4}$$

The displacement of the front of the initiating bar u_1 is the resultant of incident and reflected waves:

$$u_1(t) = c_0 \cdot \int_0^t \varepsilon^I(t)\, dt + (-c_0) \cdot \int_0^t \varepsilon^R(t)\, dt = c_0 \cdot \int_0^t (\varepsilon^I - \varepsilon^R)(t)\, dt. \tag{2.5}$$

Similarly, the displacement of the transmitting bar u_2 can be determined as follows:

$$u_2 = c_0 \cdot \int_0^t \varepsilon^T(t)\, dt. \tag{2.6}$$

Equations of front displacement velocities for each of the bars v_1, v_2 can be represented as:

$$v_1(t) = c_0 \cdot (\varepsilon^I(t) - \varepsilon^R(t)); \tag{2.7}$$

$$v_2(t) = c_0 \cdot \varepsilon^T(t); \tag{2.8}$$

where: v_1 - front speed of the initiating bar;
v_2 - front speed of the transmitting bar.

However, dependencies for forces P_1, P_2 applied to the edges of the samples are:

$$P_1(t) = E \cdot A \cdot (\varepsilon^I(t) + \varepsilon^R(t)); \tag{2.9}$$

$$P_2(t) = E \cdot A \cdot \varepsilon^T(t); \tag{2.10}$$

where: P_1 - force at the end of the initiating bar;
P_2 - force at the end of the transmitting bar.

Additionally, assuming that in a short sample the stress distribution is homogeneous throughout its entire volume, you can determine the average stress inside the sample σ as:

$$\sigma(t) = \frac{P_1(t) + P_2(t)}{2 \cdot A_0} = \pm\frac{1}{2} \cdot \frac{E \cdot A \cdot \left(\varepsilon^I(t) + \varepsilon^R(t) + \varepsilon^T(t)\right)}{A_0}; \tag{2.11}$$

where: A_0 - cross-sectional area of the sample;
A - cross-sectional area of the bars.

When we assume that:

(2.12) $$P_1(t) \cong P_2(t);$$

(2.13) $$\varepsilon^I(t) + \varepsilon^R(t) \cong \varepsilon^T(t);$$

(2.14) $$A = A_0;$$

we will get the stress equation as a function of time inside the sample σ:

(2.15) $$\sigma(t) \cong \pm E \cdot \varepsilon^T(t).$$

Average strain in the sample ε is:

(2.16) $$\varepsilon(t) \cong \pm \frac{2 \cdot c_0}{L_0} \cdot \int_0^t \varepsilon^R\,(t)\,dt;$$

where: L_0 - sample length;

and the average strain rate $\dot{\varepsilon}$ can be designated as:

(2.17) $$\dot{\varepsilon}(t) = \frac{2 \cdot c_0}{L_0} \cdot \varepsilon^R(t).$$

However, to determine the circumferential stress of the casing $\sigma_\theta(t)$, the equation must be used:

$$\sigma_\theta(t) \cong \pm E_\theta \cdot \varepsilon^\theta(t);$$

The measurement of peripheral stresses in the casing of the soil test sample is necessary to use the modified Kolsky method that allows determining the volume deformation of the tested sample and the intensity of strain. According to this modified method, the radial strain of the casing ε_r as a function of time is determined from the correlation [33]:

(2.18) $$\varepsilon_r(t) = \frac{R_2^2(1-v) + R_1^2(1+v)}{2 \cdot R_2^2} \cdot \varepsilon^\theta(t);$$

where: R_1 - outer radius of the casing;
R_2 - inner radius of the casing;
v - Poisson's ratio for the casing material.

Finally, the volume strain of the sample θ and the intensity of strain ε_i at the volumetric stressed condition are determined from the formulas:

(2.19) $$\theta = \varepsilon + 2 \cdot \varepsilon_r.$$

An intensity of strain ε_i:

(2.20) $$\varepsilon_i = \frac{2}{3}(|\varepsilon| + |\varepsilon_r|).$$

Taking into account changes in the volume deformation of the sample, the final correlations for stress and axial strain in the sample take the form:

(2.21) $$\sigma_0(t) = \sigma(t)\big(1 \pm \varepsilon(t)\big);$$

(2.22) $$\varepsilon_0(t) = ln\big(1 \pm \varepsilon(t)\big).$$

Taking into account - change of sample cross section as a function of time:

$$A(t) = \frac{A}{1 \pm \varepsilon(t)}. \tag{2.23}$$

3. FINDINGS

As a result of a series of test shots, changes in physical characteristics were obtained for each of the soil samples tested, which are presented in Table 1.

Table 1. Summary the of results of the test series.

	Soil sample moisture content			
	$w_1 = 0$ [%]	$w_2 = 4{,}6$ [%]	$w_3 = 9{,}6$ [%]	$w_4 = 14{,}6$ [%]
Sample mass before the shot m_0 $[g]$	16,00	19,92	17,76	22,28
Sample length before the shot L_0 $[mm]$	29,70	32,27	29,76	33,10
Bulk density of the soil before the shot $\rho_0 \left[\frac{g}{cm^3}\right]$	1,67	1,91	1,84	2,09
Shot pressure p $[bar]$	5,03	5,04	5,06	5,02
Bar-projectile speed $v_0 \left[\frac{m}{s}\right]$	33,22	31,45	33,11	30,77
Sample mass after the shot m_1 $[g]$	16,00	19,87	17,55	20,56
Difference in sample mass Δm $[g]$	0,00	0,05	0,21	1,72
Sample length after the shot L_1 $[mm]$	25,20	27,98	25,07	29,03
Difference in sample length ΔL $[mm]$	4,50	4,29	4,69	4,07
Bulk density of the soil after the shot $\rho_1 \left[\frac{g}{cm^3}\right]$	1,97	2,20	2,16	2,20
Difference in sample bulk density $\Delta\rho$	0,30	0,29	0,32	0,11

Below are the results of experiments in the form of diagrams based on the equations and correlations given in Section 2.3, in the first place these are the strain diagrams obtained directly from strain gauges using synchronization of the initial pulses:

- strain waveforms $\varepsilon^I(t), \varepsilon^R(t), \varepsilon^T(t), \varepsilon^\theta(t)$ for the sample $w_1 = 0$ [%], Figure 8;
- strain waveforms $\varepsilon^I(t), \varepsilon^R(t), \varepsilon^T(t), \varepsilon^\theta(t)$ for the sample $w_2 = 4{,}6$ [%], Figure 9;

- strain waveforms $\varepsilon^I(t), \varepsilon^R(t), \varepsilon^T(t), \varepsilon^\theta(t)$ for the sample $w_3 = 9{,}6$ [%], Figure 10;
- strain waveforms $\varepsilon^I(t), \varepsilon^R(t), \varepsilon^T(t), \varepsilon^\theta(t)$ for the sample $w_4 = 14{,}6$ [%], Figure 11.

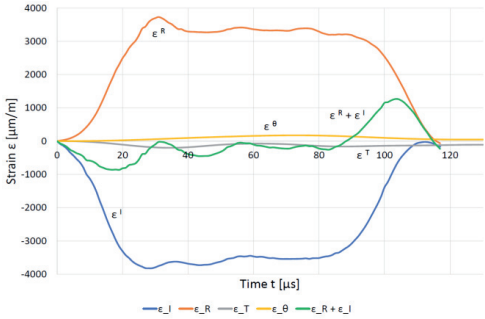

Fig. 8. List of dependencies of longitudinal strain of the bars $(\varepsilon^I, \varepsilon^R, \varepsilon^T)$ and the peripheral strain of the casing ε^θ depending on the time t - sample $w_1 = 0$ [%].

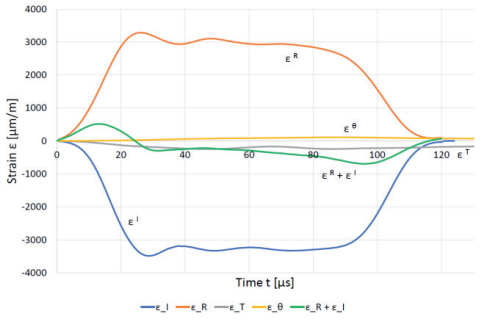

Fig. 9. List of dependencies of longitudinal strain of the bars $(\varepsilon^I, \varepsilon^R, \varepsilon^T)$ and the peripheral strain of the casing ε^θ depending on the time t - sample $w_2 = 4{,}6$ [%].

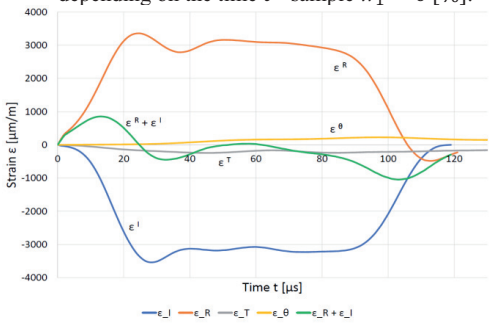

Fig. 10. List of dependencies of longitudinal strain of the bars $(\varepsilon^I, \varepsilon^R, \varepsilon^T)$ and the peripheral strain of the casing ε^θ depending on the time t - sample $w_3 = 9{,}6$ [%].

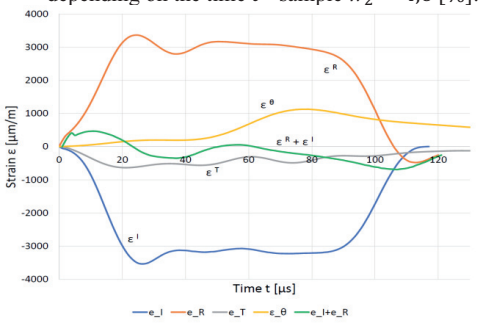

Fig. 11. List of dependencies of longitudinal strain of the bars $(\varepsilon^I, \varepsilon^R, \varepsilon^T)$ and the peripheral strain of the casing ε^θ depending on the time t - sample $w_4 = 14{,}6$ [%].

The results presented in Figures 8-11 indicate that the increase in the accuracy of the synchronization of the initial pulses allows to obtain a better approximation of the sample equilibrium state. Then, collective charts of changes in the mechanical properties of the tested soil samples are presented as a function of time:

- changes in stress in the ground σ in Figure 12;
- soil strain ε in Figure 13;
- soil strain rate $\dot{\varepsilon}$ in Figure 14.

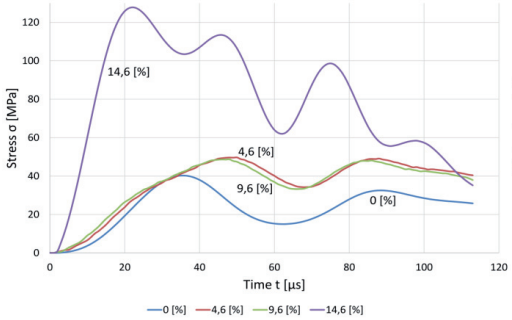

Fig. 12. List of longitudinal stress changes in the sample σ over time t.

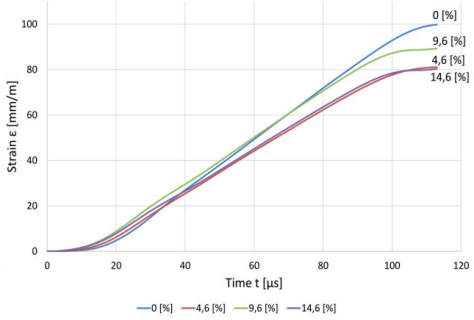

Fig. 13. List of changes in longitudinal strain of the soil samples ε as a function of time t.

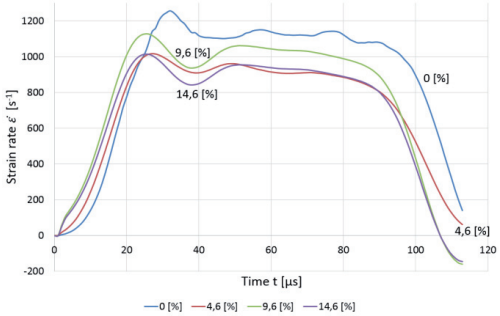

Fig. 14. A collective list of soil strain rate charts $\dot{\varepsilon}$ over time t.

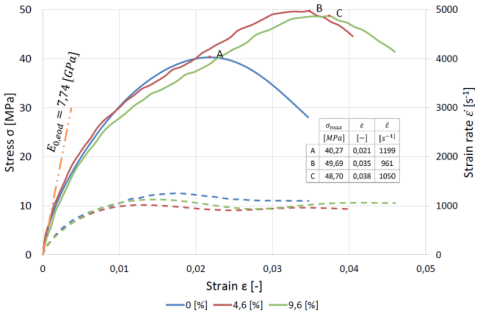

Fig. 15. Collective list of the dependence of stress - strain for the soils with less than total moisture ($w < w_{sat}$).

After testing the sample $w_4 = 14{,}6\ [\%]$ it was noticed that water splashes appeared on the bars and the casing. The exact water loss can be determined by re-measuring the sample mass after being hit by the bar-projectile - Table 1 provides information on a significant difference in mass m_0 and m_1 compared to the previous results, $\Delta m = 1{,}72\ [g]$ can be designated.

The impact of moisture content on the results obtained can be seen on the diagrams of stress changes as a function of strain. In the soil with a moisture content of less than the total ($w < w_{sat}$), the soil skeleton works under conditions of effective stress. In the water-saturated soils under dynamic loads, water with a low content air does not flow out and it works evenly with the soil skeleton. The soil works in total stress, and even water carries the load to a greater extent than the soil skeleton. Figures 15 and 16 show the curves of dynamic compression for various moisture (Fig. 15 for less than total moisture ($w < w_{sat}$), and Fig. 16 for the water-saturated soil) for silty sand soil samples

with determined values of the initial dynamic oedometric modulus $E_{0,oed}$ modulus as well as local maximum plastic stresses and corresponding strains and strain rates, i.e. points A, B, C, and D.

The course of the curves in Figures 15 and 16 is limited to the range of stress changes without the effect of reflected waves. These figures show the initial dynamic oedometric modulus. For the case of moisture $w_1 = 0\ [\%], w_2 = 4{,}6\ [\%]$ and $w_3 = 9{,}6\ [\%]$, approximately the value of $E_{0,oed} = 7{,}74\ GPa$ was determined and for the case of $w_4 = 14{,}6\ [\%]$ the value of $E_{0,oed} = 49{,}58\ GPa$ was determined.

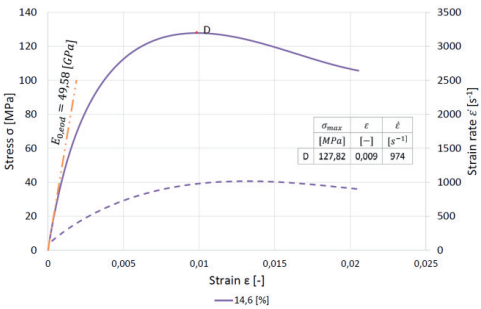

Fig. 16. Dependence of stress - strain for the water-saturated soil.

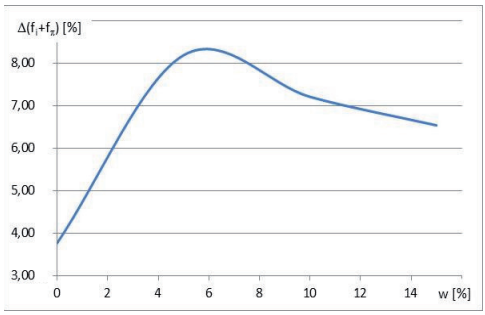

Fig. 17. Change in the content of fine fractions in the soil after the test, depending on the moisture content.

Another element analysed was the unique analysis of the change in granulation of the tested soil samples after the test. Sieve analysis was performed on the soil taken from the samples tested for all four moisture contents, two for each moisture content. The obtained amount of material allowed to perform a sieve analysis with an accuracy of 0,3 [%] of the mass content of individual fractions. The granulation curves had a similar course to the soil curve taken for testing, although some regularities consisting in changes in granulation can be observed. Figure 17 shows the dependence of the change in the content of fine fractions, understood as the sum of the content of the argillaceous fraction f_i and silty f_π after the test $\Delta(f_i + f_\pi)$ depending on the moisture content of the examined soil.

It should be noted that the course of the chart of the fine content change is similar to the course of the optimum moisture content test chart (see Figure 2).

4. DISCUSSION

By analysing summary statements of dependencies it is possible to observe that the sample $w_4 = 14{,}6\ [\%]$ with selected parameters differs in character from the results for other samples with a lower

water content. It can be suggested that the water contained in the granular soil structure for this sample carries the dynamic load equally and behaves in an elastic way at the moment of dynamic impact. The void ratio of this sample before the test was 0,43, while after the test it amounted to 0,38. The moisture content of the tested sample was higher than the total moisture content of the sample after the test, which was 14,35 [%]. In the remaining samples, in which the degree of filling the pores with water was less than 0,8, the gas (air) filling these pores at the moment of dynamic impact was not able to carry these loads. The energy is used to thicken the air voids. Table 2 below presents the physical characteristics of the samples after the test: the void ratio e, the total moisture content w_{sat} and moisture level S_r.

Table 2. Physical features of the soil with a fine fraction content of 20,5 [%] after the test.

	Initial moisture				Proctor test w_{opt}
	0,0 [%]	4,6 [%]	9,6 [%]	14,6 [%]	9,6 [%]
e	0,35	0,26	0,34	0,38	0,42
w_{sat}	13,03	9,81	13,00	14,36	16,03
S_r	0,00	0,47	0,74	1,02	0,91

It can be seen that after the test, the soil void ratio decreases in relation to that obtained in the Proctor test, which indicates dynamic soil compaction during the test using a SHPB. This compaction is lower in the absence of water in the pores, but decreases with increasing moisture content. For moisture content above optimal, the compaction of the samples is even less than for the dry soils.

To confirm the change in soil compaction under dynamic loading, additional tests were carried out for samples with a fine fraction of 2,9 [%]. Figure 18 below shows the dependence of the change in the content of fine fractions, understood as the sum of the content of argillaceous f_i and silty f_π fractions after the test $\Delta(f_i + f_\pi)$ depending on the moisture content of the examined soil.

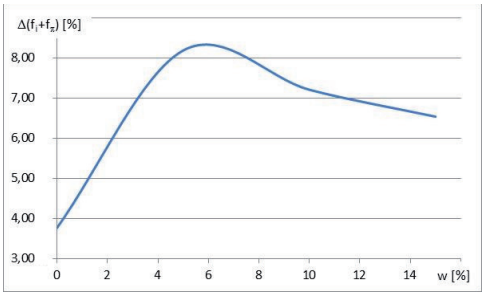

Fig. 18. Change in the content of fine fractions in the soil after the next test, depending on the moisture content.

Table 3 summarizes the physical characteristics of the soil samples with a fine fraction of 2,9 [%] after the SPHB test.

Table 3. Physical features of the soil with a fine fraction content of 2,9 [%] after the test.

	Initial moisture				Proctor test w_{opt}
	0,0 [%]	5,0 [%]	10,0 [%]	15,0 [%]	10,5 [%]
e	0,35	0,32	0,36	0,33	0,39
w_{sat}	13,34	12,15	13,47	12,53	14,76
S_r	0,00	0,38	0,71	1,17	0,71

It should be noted that the highest density of soil subjected to dynamic loading occurs at a moisture content of approximately half of the optimum moisture content.

5. SUMMARY

Experimental oedometric tests using the Split Hopkinson Pressure Bar (SHPB) to determine the dynamic behaviour for 4 ground base samples with different moisture contents ($w_1 = 0$ [%], $w_2 = 4{,}6$ [%], $w_3 = 9{,}6$ [%] and $w_4 = 14{,}6$ [%]) subjected to dynamic impact at a strain rate $\dot{\varepsilon}$ of 10^3. Silty sand soil with a fine fraction of 20,5 [%] was used for the tests. On the basis of signals from measuring strain gauges stuck on the initiating and transmitting bars and the sample casing, as well as using appropriate equations contained in the literature used, the following experimental relations were determined: soil sample stress $\sigma(t)$, its strain $\varepsilon(t)$ and strain rates $\dot{\varepsilon}(t)$, depending on the time. The obtained diagrams of strain from strain gauges allowed to receive the curves of dynamic compression for various moisture for silty sand soil samples with determined values of the initial dynamic oedometric modulus $E_{0,oed}$ as well as local maximum plastic stresses and corresponding strains.

It becomes advisable to conduct further experiments for a larger number of series of tests using the SHPB and to confirm whether the above described phenomenon of soil granulation change after the test also takes place at other contents of fine fractions. These tests should cover soils with different granulations and different moisture contents. During these tests, it is also necessary to determine the impact of the fine fraction content ($f_i + f_\pi$) and moisture content on the change in soil compaction in relation to the optimum moisture content and porosity index.

Another area for analysis is to examine the effect of moisture content on dynamic compaction. The test results obtained show that this compaction is different than in the case of the Proctor test.

REFERENCES

[1] Field, J. E., Walley, S.M., Proud, W. G., Goldrein, H. T. and Siviour, C. R. (2004). "Review of experimental techniques for high rate deformation and shock studies". *International Journal of Impact Engineering*, 30(7): 725-775.

[2] An, H.M. and Liu, L. (2019). "Numerical study of dynamic behaviors of concrete under various strain rates". *Archives of Civil Engineering*, LXV(4): 21-36.

[3] Felice, C.W., Gaffney, E.S., Brown, J.A. and Olsen, J.M. (1987). "Dynamic high stress experiments on soil". *Geotech. Test. J.,* 10: 192–202.

[4] Charlie, W.A., Ross, C.A. and Pierce, S.J. (1990). "Split-Hopkinson pressure bar testing of unsaturated sand". *Geotech. Test. J.,* 13: 291–300.

[5] Bragov, A.M., Gandurin, V.P., Grushevskii, G.M. and Lomunov, A.K. (1995). "New potentials of Kolsky's method for studying the dynamic properties of soft soils". *J. Appl. Mech. Tech. Phys*., 36: 476-481.

[6] Bragov, A.M., Grushevsky, G.M. and Lomunov, A.K. (1996). "Use of the Kolsky method for confined tests of soft soils". *Experimental Mechanics*, 36: 237-242.

[7] Bragov, A.M., Lomunov, A.K., Chmielewski, R. and Kruszka, L. (2002). „Study of dynamic properties of selected soils at high rate of loading (in Polish)". *Biuletyn WAT*, LI: 59–72.

[8] Bragov, A.M., Lomunov, A.K., Sergeichev, I.V., Tsembelis, K. and Proud W.G. (2008). "Determination of physicomechanical properties of soft soils from medium to high strain rates". *International Journal of Impact Engineering*, 35: 967–976.

[9] Martin, B.E., Chen, W., Song, B. and Akers, S.A. (2009). "Moisture effects on the high strain-rate behavior of sand". *Mech. Mater*., 41: 786–798.

[10] Song, B., Chen, W. and Luk, V. (2009). "Impact compressive response of dry sand". *Mech. Mater*, 41: 777–785.

[11] Huang, S., Chen, R. and Xia, K.W. (2010). "Quantification of dynamic tensile parameters of rocks using a modified Kolsky tension bar apparatus". *Journal of Rock Mechanics and Geotechnical Engineering*, 2(2): 162-168.

[12] Luo, H., Lu, H., Cooper, W.L. and Komanduri, R. (2011). "Effect of mass density on the compressive behavior of dry sand under confinement at high strain rates". *Experimental Mechanics*, 51: 1499–1510.

[13] Omidvar, M., Iskander, M. and Bless, S. (2012). "Stress-strain behavior of sand at high strain rates". *International Journal of Impact Engineering*, 49: 192-213.

[14] Xia, K. and Yao, W. (2015). "Dynamic rock tests using split Hopkinson (Kolsky) bar system – A review". *Journal of Rock Mechanics and Geotechnical Engineering*, 7(1): 27-59.

[15] Li, M., Mao, X., Cao, L. and Pu, H. (2017). "Influence of Heating Rate on the Dynamic Mechanical Performance of Coal Measure Rocks". *International Journal of Geomechanics*, 17(8).

[16] Lv, Y., Liu, J. and Xiong, Z. (2019). "One-dimensional dynamic compressive behavior of dry calcareous sand at high strain rates". *Journal of Rock Mechanics and Geotechnical Engineering*, 11(1): 192-201.

[17] Wen, S., Zhang, C., Chang, Y. and Hu, P. (2019). "Dynamic compression characteristics of layered rock mass of significant strength changes in adjacent layers". *Journal of Rock Mechanics and Geotechnical Engineering*, 12(2): 353-365.

[18] Xu, J., Kang, Y., Wang, Z. and Wang, X. (2020). "Dynamic Mechanical Behavior of Granite under the Effects of Strain Rate and Temperature". *International Journal of Geomechanics*, 20(2).

[19] Wang, Z. and Lu, Y. (2003). "Numerical analysis on dynamic deformation mechanism of soils under blast loading". *Soil Dynamics and Earthquake Engineering*, 23: 705-714.

[20] An, J. (2010). "Soil behavior under blast loading". Ph.D. dissertation, University of Nebraska.

[21] An, J., Yuan, C. Y., Cheeseman, B. A. and Gazonas, G. A. (2011). "Simulation of Soil Behavior under Blast Loading". *International Journal of Geomechanics*, 11(4).

[22] Anderson, C.E., Behner, T., Weiss, C.E., Chocron, S. and Bigger R.P. (2010). "Mine blast loading: experiments and simulations", Southwest Research Institute, Report 18.12544/011.

[23] Windisch, E.J. and Yong, R.N. (1970). "The Determination of soil strain-rate behavior beneath a moving wheel". *Journal of Terramechanics*, 7(1): 55-67.

[24] Gu, Q. and Lee, F.H. (2002). "Ground response to dynamic compaction of dry sand". *Geo-technique*, 52(7): 481-493.

[25] Holscher, P. and van Tol, F. (2009). "Rapid load testing on piles". *Balkema: CRC Press, Taylor and Francis Group*.

[26] Hopkinson, J. (1872). "On the rupture of iron wire by a blow". *Proc. Manchester Literary Philosophical Society*, 11: 40-45.

[27] Hopkinson, J. (1872). "Further experiments on the rupture of iron wire". *Proc. Manchester Literary Philosophical Society*, 11: 119-121.
[28] Hopkinson, B. (1914). "A method of measuring the pressure produced in the detonation of high explosives or by the impact of bullets". *Phil. Trans. R. Soc. Lond*., A213: 437-456.
[29] Kolsky, T.E. (1949). "An investigation of the mechanical properties of materials at very high rates of loading". *Proc. Phys. Soc.,* B62: 676.
[30] Guo, X., Sow, C-T., Khalil, C., Heuzé, T. and Racineux, G. (2019). "Material constitutive behavior identification at high strain rates using a direct-impact Hopkinson device." *7th International Conference on High Speed Forming (ICHSF) Germany 2016*.
[31] Couque, H. (2014). "The use of the direct impact Hopkinson pressure bar technique to describe thermally activated and viscous regimes of metallic materials." *Philosophical transactions of the Royal Society A*,. 372, 2023.
[32] Semblat, J-F., Luong, P.M. and Gary, G. (1999). "3D-Hopkinson Bar: New Experiments for Dynamic Testing on Soils." *Soils and Foundations*, 39: 1-10.
[33] Bragov, A.M., Lomunov, A.K., Konstantinov, A.Yu., Lamzin, D.A., Balandin, Vl.Vl. (2016). "Estimation of radial strain of specimen on the basis of the theoretical and experimental analysis of a technique dynamic tests of materials in a rigid ferrule (in Russian)." *Problems of Strain and Plasticity Journal*, 78 (4): 378-387.

LIST OF FIGURES AND TABLES:

EKSPERYMENTALNE BADANIE DYNAMICZNEGO ZACHOWANIA PIASKU PYLASTEGO

Słowa kluczowe: mechanika gruntu, eksperymentalne testy dynamiczne, dzielony pręt Hopkinsona, test edometryczny.

Streszczenie. Artykuł obejmuje edometryczne badania eksperymentalne z wykorzystaniem techniki pręta Hopkinsona do określenia zarówno dynamicznego zachowania jak i zmian struktury dla próbek wybranego ośrodka gruntowego o różnej wilgotności poddanych oddziaływaniu dynamicznemu. Do badania wzięto piasek pylasty (siSa) o zawartości frakcji drobnych $f_i + f_\pi$ = 20,46%. W celu zapewnienia wystąpienia jednoosiowego stanu odkształcenia badanej próbki gruntu umieszczono ją w odpowiednio przygotowanej duraluminiowej osłonie pierścieniowej. Dzięki zastosowaniu tensometrów pomiarowych na prętach inicjującym oraz transmitującym, jak również osłonie zarejestrowano różne impulsy, które następnie poddano procesowi filtracji i obróbki danych, tak aby otrzymać obrazy propagacji sprężystych fal w prętach pomiarowych i w osłonie. Wykorzystując odpowiednie równania oraz zależności zmodyfikowanej metody Kolsky'ego dla trójwymiarowego stanu naprężenia w badanej próbce określono eksperymentalne zależności charakteryzujące zachowanie się próbek gruntu o różnej wilgotności: naprężenie $\sigma(t)$, odkształcenie $\varepsilon(t)$ oraz prędkość odkształcenia $\dot{\varepsilon}(t)$ w funkcji czasu. Na tej podstawie uzyskano krzywe ściskania dynamicznego dla różnej wilgotności próbek gruntu pylastego z określonymi wartościami początkowego dynamicznego edometrycznego modułu oraz lokalnych maksymalnych naprężeń plastycznych i odpowiadających im odkształceń. Podczas powyższych eksperymentów dynamicznych z próbkami gruntów typu piasku pylastego zaobserwowano, że jego dynamiczne zagęszczenie przy dużej szybkości odkształcania jest inne niż w przypadku testu Proctora. Wynika to z większej energii zagęszczania, która dodatkowo powoduje zmianę uziarnienia poprzez niszczenie ziaren w strukturze. W pracy przedstawiono wyniki analizy zmian uziarnienia dla dwóch różnych rodzajów próbek gruntu - tego typu analizy są unikalne. W związku z tym należy kontynuować eksperymenty dla takich gruntów o różnych granulacjach i różnej wilgotności, stosując technikę prętów pomiarowych Hopkinsona, w celu potwierdzenia opisanego zjawiska w innych gruntach typu piasku pylastego, które często są podłożem gruntowym dla różnych obiektów inżynieryjnych.

Received: 13.09.2020, Revised: 22.10.2020